



Comparación de los efectos producidos por los huecos de tensión reales e ideales en un motor de inducción

Comparison of effects produced by real and ideal sags on an induction motor

Juan Camilo Urrego García¹, Wilmar Camilo Molina Gómez²,
Adolfo Andrés Jaramillo Matta³

Fecha de recepción: 5 de diciembre de 2015

Fecha de aceptación: 23 de agosto de 2016

Cómo citar: Urrego García, J. C., Molina Gómez, W. C., & Jaramillo Matta, A. A. (2016). Comparación de los efectos producidos por los huecos de tensión reales e ideales en un motor de inducción. *Revista Tecnura*, 20(Edición especial), 64-81. doi: 10.14483/udistrital.jour.tecnura.2016.SE1.a05

RESUMEN

Contexto: Muchas investigaciones se enfocan en el estudio de los efectos de los huecos de tensión sobre el Motor de Inducción (Mdl); sin embargo, la mayoría de ellos se realizan considerando huecos de tensión ideales, con caídas y recuperaciones perfectas de 90°. Esto se debe tanto a la complejidad matemática que implica modelar huecos reales, como a la falta de datos que permita caracterizarlos.

Metodología: En éste artículo se analizan las diferencias entre los efectos de los huecos de tensión reales e ideales en el comportamiento de un Mdl. Para ello se modelan 7500 huecos de tensión reales y 7500 ideales, variando su magnitud y duración; posteriormente el Mdl se somete a dichos huecos de tensión y se analiza el efecto sobre las variables: picos de corriente, picos de par y pérdidas de velocidad.

Resultados: Se obtuvieron superficies 3D de los efectos de los huecos sobre cada variable analizada del Mdl y tablas comparativas de las distancias entre dichas superficies. Finalmente se obtienen nuevos grupos de severidad con los huecos de tensión reales y se determinan los casos más relevantes de la

diferencias entre las superficies obtenidas con huecos de tensión reales e ideales.

Conclusiones: El análisis realizado a Mdl sometidos a huecos de tensión puede variar drásticamente si se consideran ideales o reales; esto se debe a que las tablas de clasificación de severidad sobre las variables analizadas (picos de corriente, picos de par y pérdida de velocidad) cambian para cada tipo de hueco. No se puede afirmar que los efectos siempre son mayores o menores con huecos reales o ideales ya que las superficies de severidad presentan diferentes puntos de cruce.

Palabras Clave: Clasificación de los huecos de tensión, Efectos producidos por los huecos de tensión, Graficas de superficies en 3D, Modelos de huecos ideales y reales, Motor de inducción

ABSTRACT

Context: Many researches have focused on the study of the effects of voltage sags on the induction motor; however, most of these studies have been performed considering ideal voltage sags, with perfect falls and recoveries of 90°. This is due, in part, to the

1 Ingeniero Eléctrico de la Universidad Distrital Francisco José de Caldas. Bogotá, Colombia. Contacto: jcurreregoc@correo.udistrital.edu.co.
2 Ingeniero Eléctrico de la Universidad Distrital Francisco José de Caldas. Bogotá, Colombia. Contacto: wcmolinag@correo.udistrital.edu.co.
3 Ingeniero Electrónico, magister en Ingeniería Electrónica, magister en Ingeniería-Énfasis en Automática, doctor en Ingeniería Electrónica, Automática y Comunicaciones. Docente de la Universidad Distrital Francisco José de Caldas. Bogotá, Colombia. Contacto: ajaramillom@udistrital.edu.co.

mathematical complexity involved in modeling real sags, and also to the lack of data to characterize a real sag.

Methodology: This paper analyzes the differences between the effects of the real and ideal sags in the behavior of an induction motor. For this analysis, we modeled 7500 real sags and 7500 ideal sags, varying their magnitude and duration. Subsequently, the induction motor is subjected to these voltage sags, and we examined the effect on the behavior of the variables: current peaks, torque peaks and velocity losses.

Results: With this analysis we developed 3D surfaces of the effects of the real and ideal sags, on each analyzed variable of the induction motor; we also made comparative tables of the distances between those surfaces. Finally, we obtained new groups of

severity with the real voltage sags, and the most relevant cases of the differences between the surfaces resulting of real or ideal voltage sags.

Conclusions: The results show that, since the severity tables on the variables (current peaks, torque peaks and loss of speed) change for each type of sag, the analysis performed on induction motors when subjected to voltage sags can vary drastically if they are considered ideal or real. On the other hand, it cannot be said that the effects are always greater or smaller with real or ideal sags, since the severity surfaces have different crossing points.

Keywords: Euclidean distance, Effects produced by sags, Ideal and real sags model, Induction motor, Sags classification, 3D surface graphs.

INTRODUCTION

Energy quality is today an interesting topic due to the effect that electric disturbs cause in electrical systems. New electrical structures concerns emphases on better and accurate power quality feeds. Sags are identified as a fall of voltage signal with short duration. Due to their frequent presence on electrical systems their severity could be worse than other kind of disturbances in electrical network.

It is well known that induction machine belongs to almost 80% of electrical industrial loads due to its special electrical and mechanical characteristics (Hedayati & Mariun, 2012). Induction motor is very sensitive to sags voltage disturbances, but also it can produce them as a consequence of severe start current. In fact, it is necessary to understand the behavior that induction motor will have when it is subjected by voltage disturbance sags.

Research has been conducted to evaluate, satisfy and improve the effects of power quality on induction motor. However the most of sag contribution studies present results based on ideal sags that in most cases do not represent real scenarios of sags effects.

A rectangle sag shape is commonly used to analyze faulty effects in electrical equipment (Caicedo, Navarro, Rivas & Santamaria, 2012) due to its facility to represent this severity, however it ignores important differences in variations of magnitude voltage along sag duration. This concern would probably change the final results. Rectangle sags could not be suitable to analyze the behavior of induction motor because important details are out of plot. Some features such as delayed voltage recovery after sag, fall slope, recover slope and peaks of short duration are ignored when ideal sags are used in the simulation of electrical systems. It is wrong to not include such parameters because the strong voltage drop caused by the impedance of the power source prevents the rapid recovery of the motor (Aree, 2012). Those effects could change the behavior of speed, torque and current if motor is subjected to ideal sags.

The differences between the effects caused by real and ideal sags on the motor dynamics are discussed in this paper, and the influences of different voltage sags classified by M. H. J. Bollen (Bollen J., 2000) will be considered to fully understand effects in correlation with the

induction motor behavior and signal profile. The three-phase symmetrical and unsymmetrical sags are discussed due to their influences on motor speed losses, current peaks and torque peaks in order to establish a mechanism of protection based on sag severity.

METHODOLOGY

Induction machine model

To test induction motor behavior under voltage sags is necessary to select a model that can apply for a widely amount of motors in electrical industrial systems. Also, accurate parameters are needed to improve propinquity of results. The selected model is the single cage, and for the estimation of its parameters the technique in (Jaramillo Matta, 2010) is used, this technique, called torque-speed tracking, begins with manufacture data and solve issues caused by missed functional points given by manufacturer. The minimized error technique estimates induction motor parameters by the calculation of missing points of torque-speed curve.

Modeling sags

The sags are defined as a voltage drop between 10% and 90% (of its nominal value), with a subsequent recovery that can last between 0.5 cycles and 1 minute. The characterization of the real sags depends on different variables, including the impedance of the system where the fault occurs and the behavior of the load (Chen & Xiao, 2012). The ignorance of these variables makes these sags are assumed as ideal, but when there are several three-phase loads connected to the affected network, the analysis using the ideal sag model does not generate reliable results. Figure 1 presents a group of three sags produced by monophasic fault and their respective rectangular ideal sag.

The ideal sags are preferably used to fault analysis because construction of those kinds of signals can be done by mathematical models; also it can approximate real behavior of equipment to voltage sags.

On the other hand, real sags do not consider a pattern easy to identify, they have different features of waveform, duration and depth. Real sags present

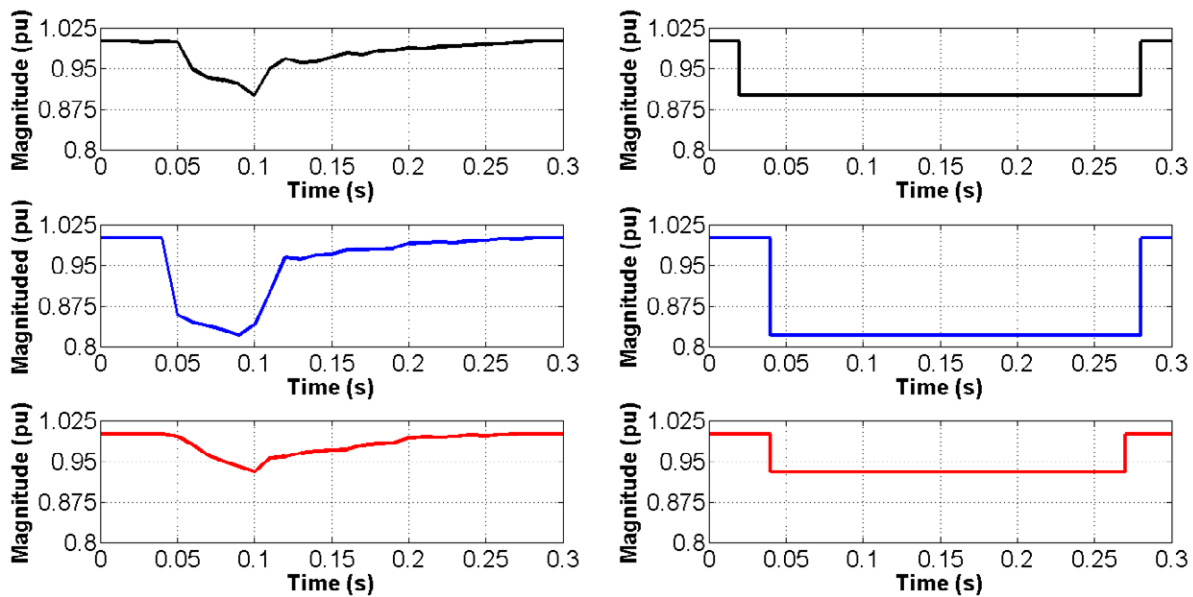


Figure 1. Real (left) vs. ideal (right) sags.

Source: own work.

different magnitudes before, during and after fault happen, they are not rectangular (Urrego, Molina y Jaramillo, 2015). As an example, figure 1 shows the difference between real and ideal sags. On the left side are three real voltage sags (in RMS value), obtained from experimental measurements with an electric power quality analyzer configured with a sampling period of 0.833 ms. The instantaneous measurement is performed according to IEC 61000-4-15. On the right side are the ideal sags corresponding to each real sag. The time equation used for ideal sags is $v(t) = v_m \times \sin(\omega_1 t)$, where v_m varies as a function of the maximum depth of the corresponding real sag and ω_1 corresponds to the network frequency (in rad/s). Modeling a sag by ideal path involves loss of information because effects produced by voltage sags are closely related to the way that voltage fall

on each phase (García Quintero, Villada Duque y Cadavid Carmona, 2011).

Sags classification

The Bollen classification is used to describe equations that represent sag types (Bollen, 2000). Table 1 depicts sag equation for each phasor response depending on type sag to represent phasor diagram. Each one is modeled and integrated in simulation scenario to handle sag variations on induction motor mains.

The severity of sags on the induction motor has been previously classified (Jaramillo Matta, Guasch Pesquer y Trujillo Rodríguez, 2015), as it can be seen in table 2, the voltage sag that produces more impact in current variable is the sag type A.

Table 1. Sags classification by M. H. J. Bollen.

Type of Sag	Sag equation	Phasor diagram
A	$V_a = V$ $V_b = -\frac{1}{2}V - \frac{1}{2}jV\sqrt{3}$ $V_c = -\frac{1}{2}V + \frac{1}{2}jV\sqrt{3}$	
B	$V_a = V$ $V_b = -\frac{1}{2} - \frac{1}{2}jV\sqrt{3}$ $V_c = -\frac{1}{2} + \frac{1}{2}jV\sqrt{3}$	

Type of Sag	Sag equation	Phasor diagram
C	$V_a = 1$ $V_b = -\frac{1}{2} - \frac{1}{2}jV\sqrt{3}$ $V_c = -\frac{1}{2} + \frac{1}{2}jV\sqrt{3}$	
D	$V_a = V$ $V_b = -\frac{1}{2}V - \frac{1}{2}jV\sqrt{3}$ $V_c = -\frac{1}{2}V + \frac{1}{2}jV\sqrt{3}$	
E	$V_a = 1$ $V_b = -\frac{1}{2}V - \frac{1}{2}jV\sqrt{3}$ $V_c = -\frac{1}{2}V + \frac{1}{2}jV\sqrt{3}$	
F	$V_a = V$ $V_b = -\frac{1}{3}j\sqrt{3} - \frac{1}{2}V - \frac{1}{6}jV\sqrt{3}$ $V_c = +\frac{1}{3}j\sqrt{3} - \frac{1}{2}V + jV\sqrt{3}$	
G	$V_a = \frac{2}{3} + \frac{1}{3}V$ $V_b = -\frac{1}{3} - \frac{1}{6}V - \frac{1}{2}jV\sqrt{3}$ $V_c = -\frac{1}{3} - \frac{1}{6}V + \frac{1}{2}jV\sqrt{3}$	

Source: Bollen, 2000.

Comparison between effects produced by ideal and real sags

The variables analyzed in this paper are current peaks, torque peaks and loss speed. For those variables studies exposed that induction motor effects are very sensitive to short interruptions and voltage sags (Bollen, Hager & Roxenius, 2003; Guasch Pesquer, Córcoles, & Pedra, 2000; Guasch Pesquer, Córcoles, & Pedra, 2004; Pedra, Sainz, & Córcoles, 2007). To analyze the differences among the effects of ideal and real voltage sags, surface graphics are built to depict current peaks, torque and speed loss in function of magnitude and duration. The procedure consists in studying large sags data which belong at same sag type, for each sag peak current was located to build a main matrix that host and relate peak current vs. depth and duration plot.

Table 2. Classification of sags according to severity. Group 1 = High, and Group 4 = Low severity.

Sag type	Severity Group		
	I	T	S
A	1	3	1
B	3	4	4
C D	2	1	3
E F G	2	2	2

Source: (Jaramillo Matta, Guasch Pesquer & Trujillo Rodríguez, 2015).

Procedure

The Euclidean distance (D) is used to measure gap between ideal surface plot and real surface plot, it determines difference trough a normalize sum which link all points over 3D plot, equation (1).

$$D(SI, SR) = \sqrt{\sum_{i=1}^p \sum_{j=1}^d [sI(i, j) - sR(i, j)]^2} \quad (1)$$

The distances are normalized regarding to a reference distance for each variable, current peaks

equation (2), torque peaks equation (3), and speed losses equation (4).

$$D_{REF,I} = D(I_{MAX,h}, 0) = \sqrt{\sum_{i=1}^{25} \sum_{j=1}^{25} [I_{MAX,h}(i, j) - 0]^2} \quad (2)$$

$$D_{REF,\Gamma} = D(\Gamma_{MAX,h}, 0) = \sqrt{\sum_{i=1}^{25} \sum_{j=1}^{25} [\Gamma_{MAX,h}(i, j) - 0]^2} \quad (3)$$

$$D_{REF,\omega} = D(\omega_{MIN,h}, 0) = \sqrt{\sum_{i=1}^{25} \sum_{j=1}^{25} [\omega_{MIN,h}(i, j) - 0]^2} \quad (4)$$

Normalized sum is used to study similar facts among ideal and real sags. Furthermore it identifies differences between voltage sags types.

The normalized distances (D) between surfaces of current peaks equation (5), torque peaks equation (6) and speed losses equation (7) generated by real sags and ideal sags are calculated as follows:

$$d(I_{qh}, I_{qh}) = \frac{100}{D_{REF,I}} \sqrt{\sum_{i=1}^{25} \sum_{j=1}^{25} [I_{Xh}(i, j) - I_{Yh}(i, j)]^2} \quad (5)$$

$$d(\Gamma_{qh}, \Gamma_{qh}) = \frac{100}{D_{REF,\Gamma}} \sqrt{\sum_{i=1}^{25} \sum_{j=1}^{25} [\Gamma_{Xh}(i, j) - \Gamma_{Yh}(i, j)]^2} \quad (6)$$

$$d(\omega_{qh}, \omega_{qh}) = \frac{100}{D_{REF,\omega}} \sqrt{\sum_{i=1}^{25} \sum_{j=1}^{25} [\omega_{Xh}(i, j) - \omega_{Yh}(i, j)]^2} \quad (7)$$

Where X is the typology of sag analyzed (A, B, C, D, E, F, G); Y can be the typology of sag analyzed (A, B, C, D, E, F, G) or the matrix of maximum values for each variable (IMAX,h, Γ MAX,h y ω MIN,h) according to the case, and h indicates whether it is real (R) or ideal (I). These distances are calculated for real and ideal sags independently.

As an example, in figure 2 the current peaks surface plot of different voltage sags within

different equidistant durations is shown in logarithmic scale.

To calculate the distance between ideal and real sag surfaces, it takes as reference the distance from surface generated by ideal sag above null surface for each variable (current equation (8), torque equation (9) and speed loss equation (10)).

$$D_{REF,I\ ideal} = D(I_{q,I}, 0) = \sqrt{\sum_{i=1}^{25} \sum_{j=1}^{25} [I_{qI}(i, j) - 0]^2} \quad (8)$$

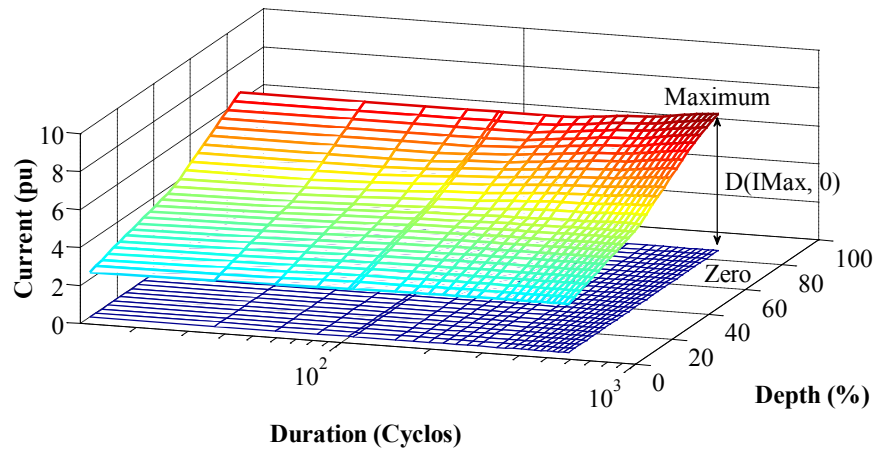
$$D_{REF,\Gamma\ ideal} = D(\Gamma_{q,I}, 0) = \sqrt{\sum_{i=1}^{25} \sum_{j=1}^{25} [\Gamma_{qI}(i, j) - 0]^2} \quad (9)$$

$$D_{REF,\omega\ ideal} = D(\omega_{q,I}, 0) = \sqrt{\sum_{i=1}^{25} \sum_{j=1}^{25} [\omega_{qI}(i, j) - 0]^2} \quad (10)$$

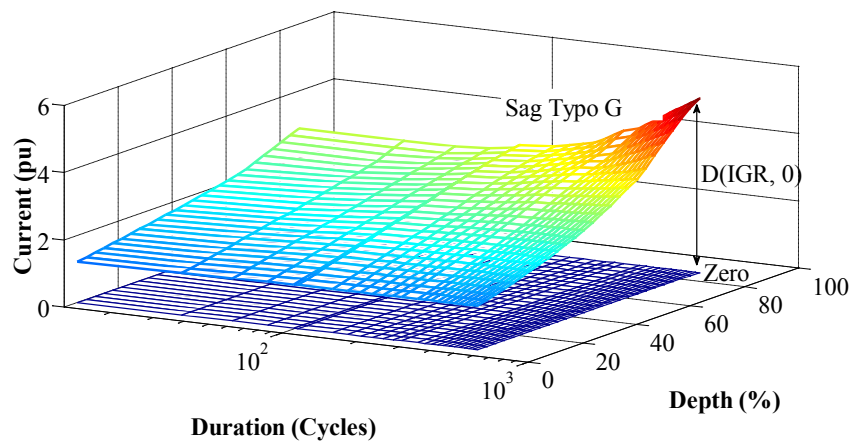
The normalized distances between surfaces are calculated based on following equations (11), (12) and (13):

$$d(I_{qI}, I_{qR}) = \frac{100}{D_{REF,I\ ideal}} = \sqrt{\sum_{i=1}^{25} \sum_{j=1}^{25} [I_{qI}(i, j) - I_{qR}(i, j)]^2} \quad (11)$$

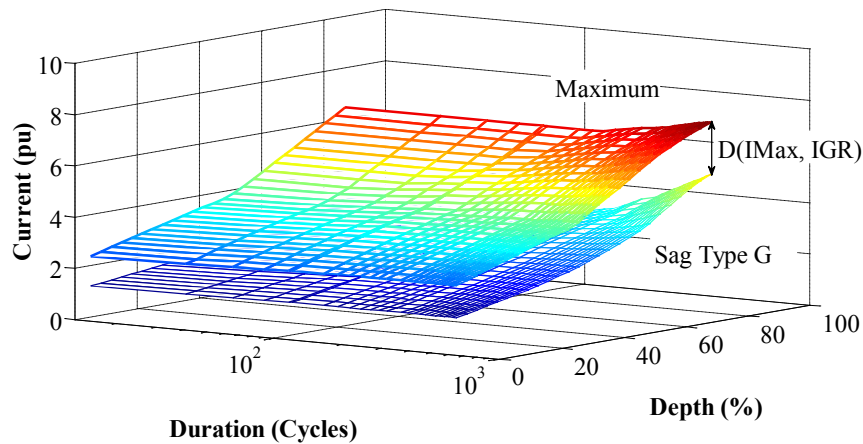
$$d(\Gamma_{qI}, \Gamma_{qR}) = \frac{100}{D_{REF,\Gamma\ ideal}} = \sqrt{\sum_{i=1}^{25} \sum_{j=1}^{25} [\Gamma_{qI}(i, j) - \Gamma_{qR}(i, j)]^2} \quad (12)$$



(a)



(b)



(c)

Figure 2. Peak currents surfaces generated by real sags. Matrix of Euclidean distance from: (a) Maximum values to null matrix, (b) Values obtained from G sag type to zero matrix, (c) Maximum values to values from G sag type.

Source: own work.

$$d(\omega_{qI}, \omega_{qR}) = \frac{100}{D_{REF, ideal}} = \sqrt{\sum_{i=1}^{25} \sum_{j=1}^{25} [\omega_{qI}(i, j) - \omega_{qR}(i, j)]^2} \quad (13)$$

Figure 3 shows the distance between the surface of current peaks that generates ideal sag type G and

current peaks surface that generates real sag type G.

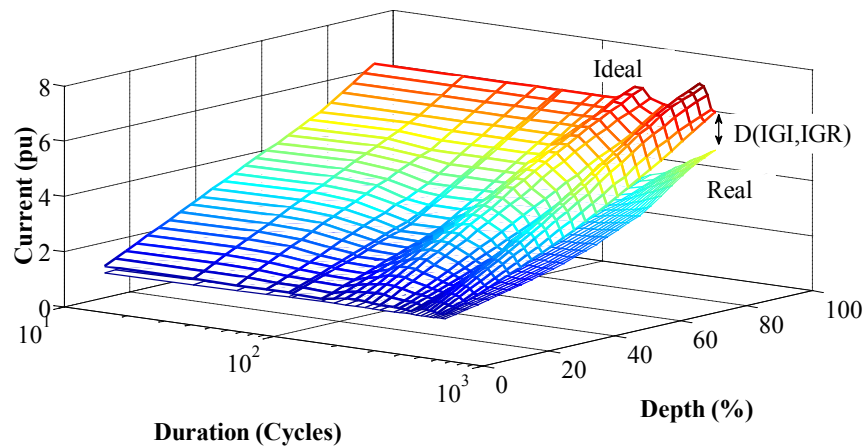


Figure 3. Distance between current peak surfaces for real and ideal sags type G.

Source: own work.

RESULTS

Induction machine model

Induction machine model used is showed in figure 4; also electrical parameters calculated by torque-speed tracking are depicted in table 3. The specifications of selected induction machine are as follows: P = 75 kW, VL = 3,3 kV, frequency = 50 Hz, nm = 1455 r/min.

Table 3. Parameters estimated by torque-speed tracking technic.

P (KW)	r_s	X_{sd}	X_m	X_{rd}	r_r
75	0,098	0,155	4,127	0,155	0,077

Source: Jaramillo Matta, 2010.

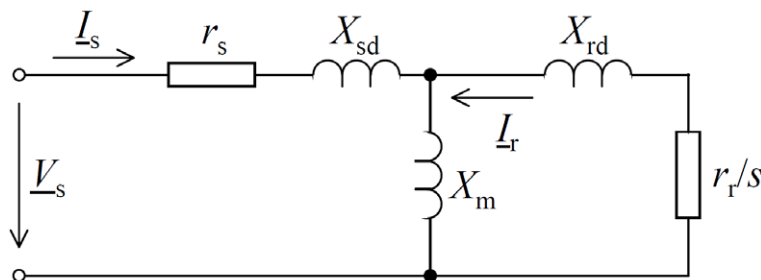


Figure 4. Steady state equivalent circuit of induction machine.

Source: Guasch Pesquer, 2006.

Assuming stator inductances $L_{sa} = L_{sb} = L_{sc} = L_s$, rotor inductances $L_{ra} = L_{rb} = L_{rc} = L_r$, same way stator resistances R_s and rotor resistances R_r . The equations (14), (15) and (16) represent electrical behavior of induction machine:

$$[v] = [R][i] + \frac{d}{dt}[\phi] \quad (14)$$

$$\begin{bmatrix} v_s \\ v_r \end{bmatrix} = \begin{bmatrix} R_s & 0 \\ 0 & R_r \end{bmatrix} [i] + \frac{d}{dt} \begin{bmatrix} \phi_s \\ \phi_r \end{bmatrix} \quad (15)$$

The ratio among magnetic fluxes and currents is equation (16):

$$\begin{bmatrix} \phi_s \\ \phi_r \end{bmatrix} = \begin{bmatrix} M_{ss} & M_{sr} \\ M_{rs} & M_{rr} \end{bmatrix} \begin{bmatrix} i_s \\ i_r \end{bmatrix} \quad (16)$$

Understanding that the M_{sr} matrix (coupling coefficient matrix of the flow created by the rotor windings and concatenated by the stator coils) is equal to the M_{rs} matrix (coupling coefficient matrix of the streams created by the stator coils and concatenated to the rotor windings), it leads to the follow torque equation (17):

$$(t) = [t_s]^t \left\{ \frac{\partial}{\partial \theta} [M_{sr}(\theta)] \right\} [i_r] \quad (17)$$

Due to the dependency of equation (17) with θ , workload-calculating time would increase, and it cannot be calculated if basic methods of differential equation solution are used. To solve this problem, the Ku transformation is implemented (Bort, 2002) to convert complex and variable coefficient into lineal constants coefficients, thus supposing that mechanical speed is constant and magnetic circuit is lineal.

Real sags model

Modeling a real sag by mathematical function with polynomial regression technique would suppose a loss of important information. To illustrate this, Figure 5. shows a real sag and its approximation (calculated) by 50 grade polynomial regression using the "polyfit()" function of Matlab.

A large polynomial ranges are tested to choose best accurate mathematical sag model, the calculated model approximates to real model, however features as fall slope, recover slope, minimum descent point and start point change from real model to mathematical expression.

Figure 5 shows short peaks presented in real sag signal which are not drawn by the mathematical model.

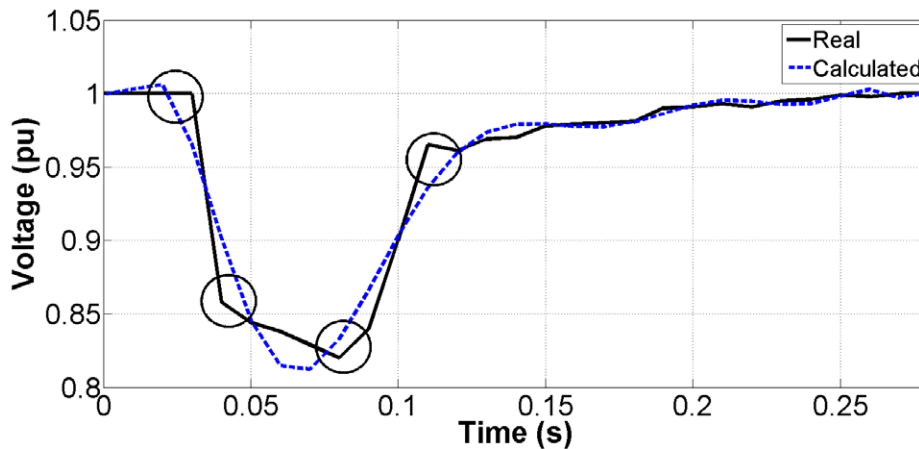


Figure 5. Mathematical sag model obtained from 50 grade polynomial regression and sag measured by signal analyzer.

Source: own work.

In order to avoid those troubles, the model is obtained by electrical signal analyzer with resolution of 0.833 ms; an interpolation technique was applied to obtain 200 samples per cycle. From 12 three-phase real sag samples within different magnitudes, durations and shapes, 1500 sags were obtained (7500 real and 7500 ideal sags). As an example, figure 6 shows variations of depth of real sag and its respective ideal sag.

For the simulations and the analysis performed in this work, 1500 holes were generated as follows: depth parameter has 25 intervals, which are varied from 10% to 90% of the maximum voltage value, and duration parameter has 25 intervals, which are varied between 0.26 seconds and 11 seconds (framed within the IEEE 1159 standard), for a total of 7500 real sags (25 durations x 25 depths x 12 holes) and 7500 ideal sags.

Comparison between effects produced by ideal and real sags

Because differences between effects need to be measured, the procedure consists on calculation of distance from surfaces generated by ideal sags to real sags, for each sag topology, on the variables: current peaks, speed losses and torque peaks obtained in simulations. Overall results can be checked in follow items:

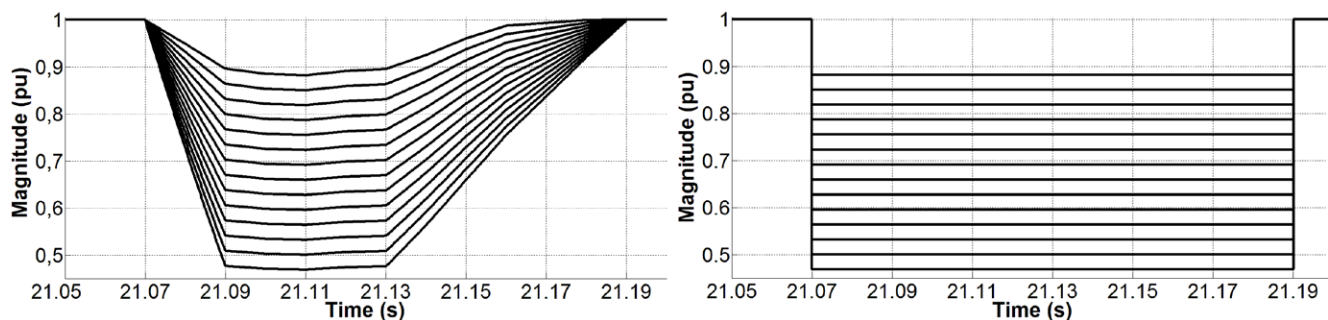


Figure 6. Variation of depth for real and ideal sag.

Source: own work.

Current peaks

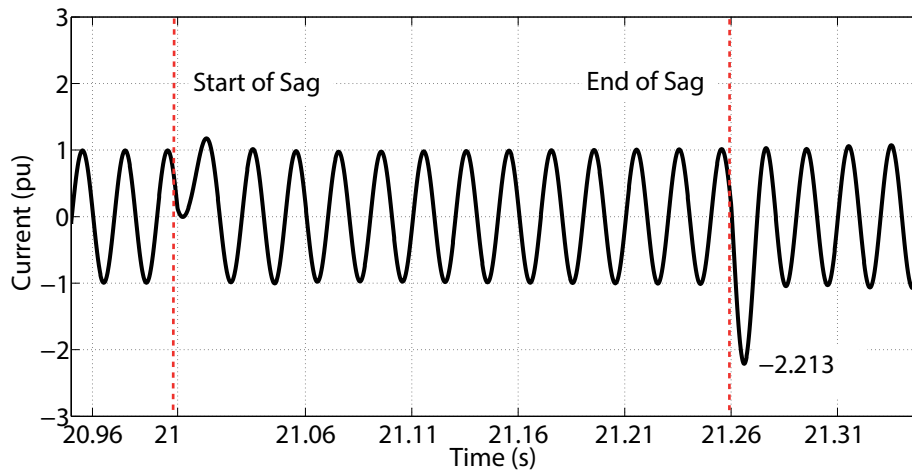
In table 4 it is identified that sags types A and G present normalized distances between 40% y 42%, the results showed that those sags have the major differences compared with the rest of topologies. In other side, voltage sag B, C, D, E and F present normalized distance under 19%, being sags type C those which reached the minor distance.

Table 4. Normalized distances between surfaces of current peaks obtained with real (R) and ideal (I) voltage sag.

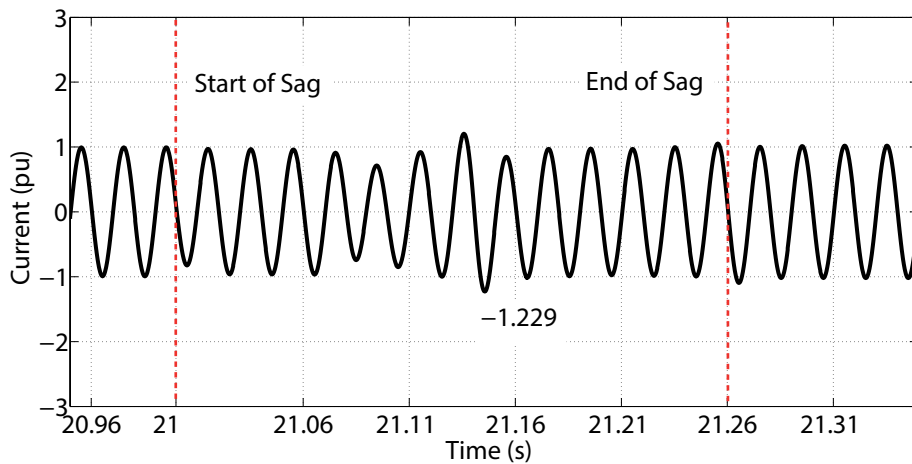
Ideal vs. real	(% PU)
IA	42,41
IB	18,83
IC	14,40
ID	14,71
IE	14,74
IF	17,27
IG	40,58

Source: own work.

For ideal sags, figure 7(a) shows current peaks at the start point and end of sag. However, for real voltage sag, figure 7(b) illustrates the current peaks that occurs during sag transition.



(a)



(b)

Figure 7. Time evolution of motor current in the most unfavorable phase (phase C) when it is subjected to ideal (a) and real (b) C voltage sag with depth of 10% and duration of 13 cycles.

Source: own work.

Torque peaks

The most important differences are presented in table 5. The major differences on torque peaks are obtained with sags types A, E and G; for those sags the distances vary from 29% to 42%. Results obtained with sags type D present minor differences due to normalized distance of 9.5%, therefore their effects can be considered similar.

Table 5. Normalized distances between surfaces of torque peaks obtained with real (R) and ideal (I) voltage sag.

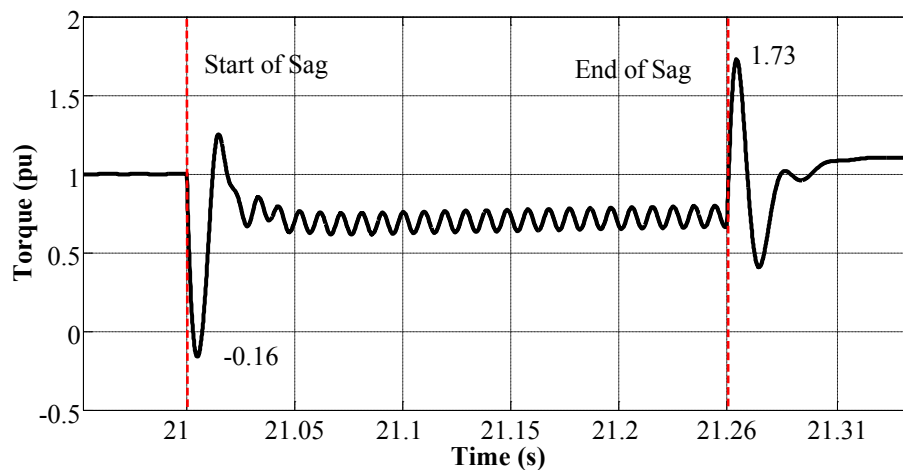
Ideal vs. real	(% PU)
ΓA	29,97
ΓB	20,25
ΓC	18,87
ΓD	9,548
ΓE	40,88
ΓF	13,25
ΓG	42,10

Source: own work.

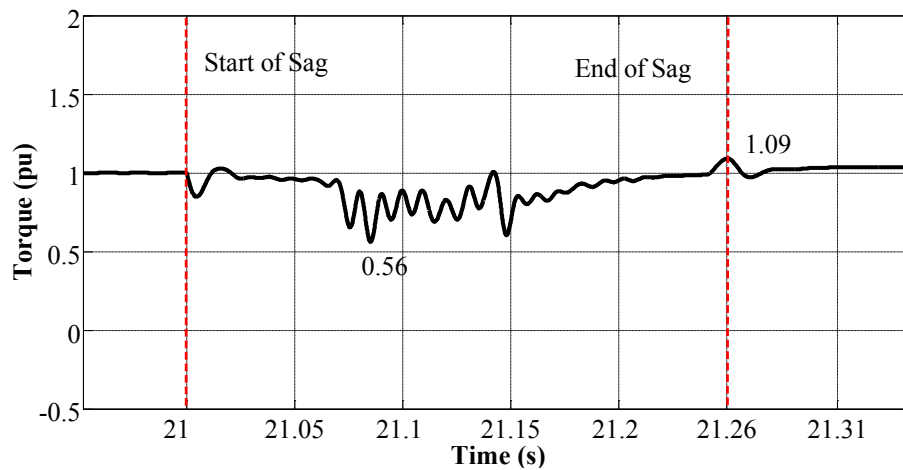
Torque response is similar to those identified in current peaks under ideal voltage sag, torque peaks occur at start and voltage recovery points, whereas in real sags, torque peaks occur during the transition of sag, these are less severe than those with ideal sag, figure 8; furthermore the waveform of torque signal depends primarily on the characteristics of voltage sag shape that is submitted to the induction motor.

Speed losses

For speed losses, sags types B and E present the bigger normalized distance. Sag types A and C present differences from 0,5%, as showed in table 6. Sag types D, F and G sags present little differences in the distances, around zero, so their effects can be considered similar.



(a)



(b)

Figure 8. Torque signal evolution obtained by A ideal sag type (a) and A real sag type (b) within 10% of depth and 13 cycles.

Source: own work.

As a conclusion, the differences of speed losses caused by real and ideal voltage sags are not relevant; figure 9 shows a very similar response in loss speed behavior.

Severity groups

The severity of the effects is compared among sag typologies based on effects on current peaks, torque peaks and speed losses. An induction motor is subjected to all variation of sags designed, results are classified in table 7 where severity is categorized in three levels: high, medium and low.

Table 6. Normalized distances between surfaces of speed losses obtained with real (R) and ideal (I) voltage sag.

Ideal vs. real	(% PU)
ωA	0,536
ωB	0,908
ωC	0,530
ωD	0,103
ωE	0,874
ωF	0,192
ωG	0,210

Source: own work.

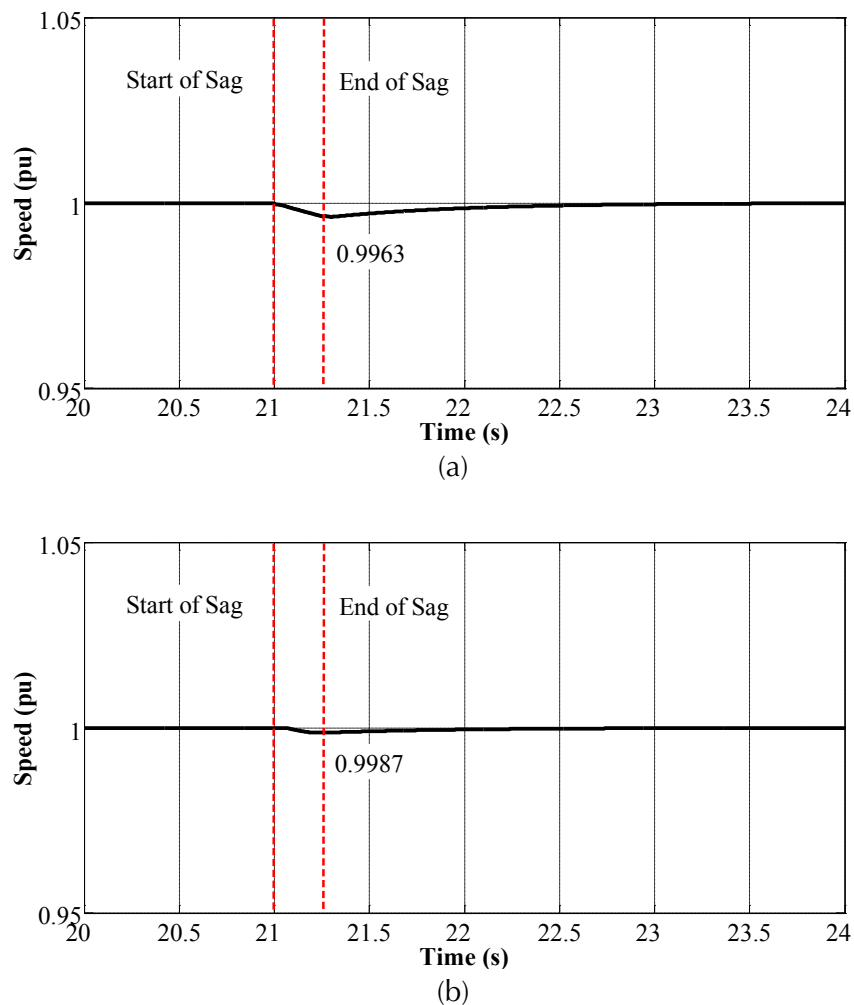


Figure 9. Speed losses caused by ideal sag type A (a) and real sag type A (b) for 10% of depth and duration of 13 cycles.

Source: own work.

As showed in table 7, there is an evident difference between current peaks surfaces generated by real sags respect to those generated by ideal sags. The most severe effects in current are obtained when motor is subjected to an ideal sag type A, the less effect is obtained with sags type B and D. In other side, when motor is analyzed with real sags, the most severe effects in current peaks are obtained with sags type E, the less severity is obtained with sags type G.

A summary of results obtained for each surfaces comparison between ideal and real cases are shown in table 8, they are categorized in three levels which determine the highs, mediums and lows differences according to normalized distance measured in % PU.

As shown in table 8, the biggest differences for current are presented with sags types A and G, therefore an analysis with ideal sags could be wrong if it is analyzed as the same way that with real sags on motor behavior. The most relevant differences for torque variable are presented when motor is

subjected to sags types G, E and A, their normalized distance between surfaces are 42,1% PU, 40,88% PU and 29,9% PU, respectively.

The consolidated results obtained from speed losses when the motor is subjected to ideal and real sags are similar; both cases do not have relevant differences because normalized distance never exceeds the 1% PU.

Crosses between 3D surfaces

According to results almost all cases show that ideal sags are more severe than real sags, however, in some cases crosses between the surfaces were presented (Figure 10), this shows that not in all cases the effects presented by ideal sags are more severe than those generated by real sags. Figure 10 shows the crosses of current peaks surfaces obtained with real and ideal sags type D for different variations of depth and duration.

Table 7. Severity of voltage sags for current peaks (IP), torque peaks (TP) and speed losses (ω_P) for real (R) and ideal (I) voltage sags.

Variable Severity	I_p, I	I_p, R	Γ_p, I	Γ_p, R	ω_p, I	ω_p, R
High	A	E	A, E, G	A	A	B, E
Medium	C, E F, G	C, F A, B, D	D, F	D, E, F, G	E, F, G	A, C
Low	B, D	G	B, C	B, C	B, C, D	D, F, G

Source: own work.

Table 8. Summary of the largest distances between surfaces of current peaks (I), torque peaks (T) and speed losses (ω) obtained with real and ideal voltage sags.

Variable Level of differences	I_{Pico}	Γ_{Pico}	ω_{Pico}
High	A, (42,41 % PU) G, (40,58 % PU)	G, (42,10 % PU) E, (40,88 % PU) A, (29,97 % PU)	B, (0,908 % PU) E, (0,874 % PU)
Medium	B, (18,83 % PU) F, (17,27 % PU)	B, (20,25 % PU) C, (18,87 % PU)	A, (0,536 % PU) C, (0,530 % PU)
Low	E, (14,74 % PU) D, (14,71 % PU) C, (14,40 % PU)	F, (13,25 % PU) D, (9,548 % PU)	G, (0,210 % PU) F, (0,192 % PU) D, (0,103 % PU)

Source: own work.

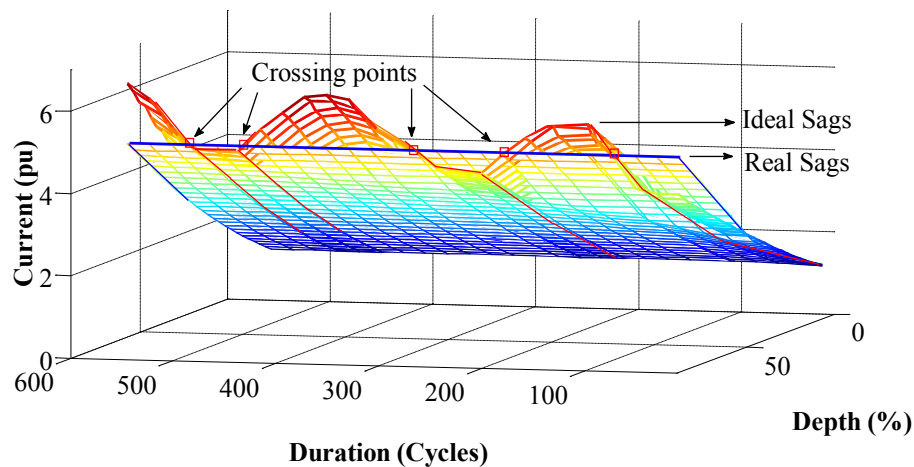


Figure 10. Crosses of current peaks surfaces obtained with real and ideal sags type D.

Source: own work.

As can be seen, surfaces not only cross at specific points but at intersections that generate areas of depth and duration, with no defined shape, where in some cases ideal sags have more severe effects and other less severe effects. As can be seen, surfaces not only cross at specific points but at intersections that generate areas of depth and duration, with no defined shape, where in some cases ideal sags have more severe effects and other less severe effects. This allows to conclude that it is not possible to determine if the effects are more severe with real or ideal sags, or to find a relation between the severity of effects and the real or ideal sags, for this a particular analysis of each case is required.

CONCLUSIONS

In this paper the comparative analysis between effects of real and ideal sags on single cage induction motor were obtained, analyzed and classified. An algorithm was designed to record changes presented in current and torque peaks, as well as speed losses of an induction motor based on type, duration and depth of real and ideal sags.

Speed losses are quite similar when motor is subjected to real and ideal sags. In the most of cases

they do not exceed 10% of nominal signal, typically over-speed protections of induction motors act for periods beyond to two minutes sustained above 25% of synchronous speed, so the signal decreasing is not relevant on the current study made.

The biggest differences in torque were found with real and ideal sags types A, E and G. The effects obtained are harmful to motor because thermal stress produced exceeds the operating conditions suggested by manufacturer. However, induction motor may have more severe effects if analysis is performed with ideal sags according to results.

The biggest differences in current were found between surfaces generated by both real and ideal sags, they were obtained with sags types A and G, normalized distances for those were 42,41% and 40,58% PU, respectively. Percentages let to discuss that accuracy of overcurrent detection devices based on ideal sags can vary around 40% in those cases, it was verified in more cases that current peaks exceeded by more than 20% of the maximum current measured at startup so it will carry that protection devices based on ideal sags could ignore the overcurrent originated due to short duration.

3D surfaces were generated and compared for all sags variations, ideal surfaces have higher values

than real surfaces in the most cases. It means that mostly, effects are more severe if the analysis on induction motor is subjected to ideal sags. However, in two current peaks surfaces (sag types D and F) and two cases of torque peaks (sag types C and F), ideal and real surfaces intersect each other in some places, this particularity leads to the conclusion that there are some areas of depth vs. duration, where effects produced by real sags are higher than those produced by ideal sags.

FUTURE PROJECTS

According to reasearch made, further research may be continued. Is the case of the design of differential protection for induction motors based on sag topology, due the knowlegment of the sags that have the worst effects on the analyzed variables; another one is the influence of start and final point of wave of a real voltage sag, because the effect could be different according the angle when the sag starts; the effects of short voltage peaks by using the single cage induction motor model, due the possible resultant transient. The influence of slope of fall and recover of real sags and the on-line determination of the sag type, for derivative control; and the effects of real and ideal sags by using the doble cage induction motor model, since being a model with different adjustment in other zones of operation, it could be obtained different results for automation and control applications.

FINANCE SUPPORT

Universidad Distrital Francisco José de Caldas (Colombia), research project titled "Efecto de las perturbaciones en la calidad de energía eléctrica sobre el motor de inducción trifásico. etapa i: huecos de tensión, sistema de tensiones desequilibrado y generación de armónicos". It belongs to convocatory 8-2013, through CIDC (Research and Development Sientific Center), Engineering Faculty, academy research group LIFAE.

REFERENCES

- Aree, P. (2012). Effects of Large Induction Motors on Voltage Sag. *Power and Energy Engineering Conference (APPEEC)*. Asia-Pacific: IEEE.
- Bollen J., M. H. (2000). Voltage Sags Characterization. En: M. H. Bollen, *Understanding Power Quality Problems: Voltage Sags and Interruptions*. Wiley-IEEE Press.
- Bollen J., M. H.; Hager, M., & Roxenius, C. (2003). Effect of induction motors and other loads on voltage dips: theory and measurements. *Power Tech Conference Proceedings*. Bologna: IEEE.
- Bort, J. V. (2002). *Estudio del Modelo Matemático del Motor de Inducción Trifásico*. Tarragona: Universitat Rovira I Virgili.
- Caicedo N. J. E.; Navarro J. L. F.; Rivas T. E., & Santamaría P. F. (2012), Simulation of voltage sag characteristics in power systems. *Revista Tecnura*, Universidad Distrital Francisco José de Caldas, 17.
- Chen, L., & Xiao, X. (2012). Voltage sags frequency assessment considering the coordination of protection system. *Harmonics and Quality of Power (ICHQP)*. 15th International Conference. Hong Kong: IEEE.
- García Quintero, E.; Villada Duque, F., & Cadavid Carmona, D. (2011). Nuevo factor para la caracterización de huecos de tensión. *Revista Facultad de Ingeniería Universidad de Antioquia*, 12.
- Guasch Pesquer, L. (2006). *Efectos de los huecos de tensión en las máquinas de inducción y en los transformadores trifásicos*. Catalunya: Universitat Politècnica de Catalunya.
- Guasch Pesquer, L.; Córcoles, F., & Pedra, J. (2000). Effects of unsymmetrical voltage sag types E, F and G on induction motors. *Harmonics and Quality of Power. Proceedings. Ninth International Conference*. Orlando, FL: IEEE.
- Guasch Pesquer, L.; Córcoles, F., & Pedra, J. (2004). Effects of symmetrical and unsymmetrical voltage sags on induction machines. *Power Delivery, IEEE Transactions*.
- Hedayati, M., & Mariun, N. (2012). Assessment of different voltage sags on performance of induction

motors operated with shunt FACTS. *Power Electronics and Drive Systems Technology (PEDSTC)*. Tehran: IEEE.

Jaramillo Matta, A. A. (2010). *Estimación de parámetros y efectos de los huecos de tensión en la máquina de inducción trifásica*. Tarragona: Universitat Rovira i Virgili.

Jaramillo Matta, A. A.; Guasch Pesquer, L., & Trujillo Rodríguez, C. L. (2015). Classification of voltage sags according to the severity of the effects on the induction motor. *DYNA*.

Pedra, J.; Sainz, L., & Córcoles, F. (2007). Effects of symmetrical voltage sags on squirrel cage induction motors. *Generation, Transmission & Distribution, IET*.

Urrego, J.; Molina, W., & Jaramillo, A. (2015). Effects produced by real sags on an induction motor. *Revista Tecnura*. Universidad Distrital Francisco José de Caldas, 19 (CITIE).

